Modeling Ultra-high Frequency Radiation Emission in PIC Codes

M. Pardal[1], A. Sainte-Marie[1], A. Reboul-Salze[1], J. Vieira[1], R.A.Fonseca[1,2]

[1] *GoLP/Instituto de Plasmas e Fusão Nuclear, Instituto Superior Técnico, Universidade de Lisboa, Lisbon, Portugal,*

[2] *DCTI/ISCTE, Instituto Universtitário de Lisboa, Lisbon, Portugal*

Introduction

From the mysterious γ ray bursts, which can be studied through the spatiotemporal structure of the radiation we receive, to the creation of sources of x-rays capable of probing nanoscale structures, radiation emission by relativistic charges is a key research field in plasma physics.

The processes behind radiation emission in plasmas result from strongly non-linear many body interactions which involve relativistic effects, so they are best modeled through Particle-In-Cell (PIC) simulations. However, capturing this radiation directly in PIC simulations is very challenging due to the large disparity between the temporal and spatial scales associated with such phenomena. Current algorithms only describe radiation processes in the Fourier space (e.g. JRAD [1]), missing the spatiotemporal features of the emitted radiation, which is crucial to many fields, such as super-resolution microscopy [2] and astrophysics [3].

Background

The radiation emitted by the plasma is the superposition of the radiation emitted by each of its charged particles. The electric (**E**) and magnetic (**B**) field associated with the radiation of a relativistically moving charge is given by [4]:

$$\mathbf{E}(\mathbf{x},t) = e\left[\frac{\mathbf{n}-\beta}{\gamma^2(1-\beta\cdot\mathbf{n})^3R^2}\right]_{\mathrm{ret}} + \frac{e}{c}\left[\frac{\mathbf{n}\times[(\mathbf{n}-\beta)\times\dot{\beta})]}{(1-\beta\cdot\mathbf{n})^3R}\right]_{\mathrm{ret}}, \qquad \mathbf{B}(\mathbf{x},t) = [\mathbf{n}\times\mathbf{E}]_{\mathrm{ret}} \tag{1}$$

e is the charge of the electron, c is the speed of light and γ is the Lorentz factor. The remaining quantities are defined as shown in Figure 1 below. β is therefore the normalized velocity of the electron, $\dot{\beta}$ its normalized acceleration, $\mathbf{n}$ is the observation direction and R is the observation distance.

In this work, we focused on developing a diagnostic that was able to capture the electromagnetic fields of the emitted radiation in a given region of space and time (called a *detector*). As the plasma is generally not in the same place as the detector, the field produced at $t = t_0$ will only reach the detector at $t = t_0 + Rc$, this way, in order to calculate $\mathbf{E}(\mathbf{x},t)$ all quantities must be evaluated at the *retarded time of emission*, t_{ret}.

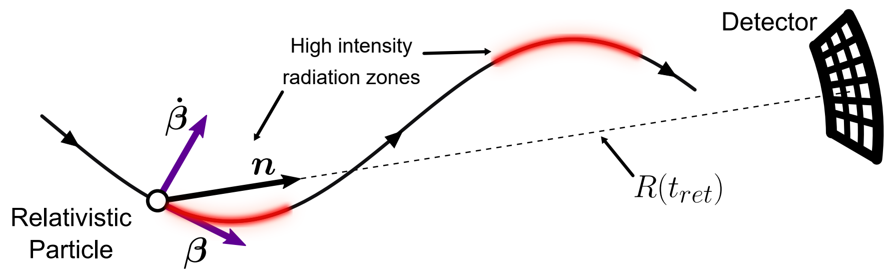

Figure 1: *Illustration of the geometry of the radiation emission process and relevant quantities. The relativistic particle follows a sinusoidal trajectory. Higher intensity is obtained with transverse acceleration.*

Post-Processing Tool

Given a set of particles' trajectories containing information about their charge, position and momentum at each time step, the post processing diagnostic uses equation (1) to compute the electric field at the detector. As stated above, the detector can be loosely defined as a finite region of space and time. With this in view, we implemented two types of detectors, a *cartesian* one, where the spatial region is defined using cartesian coordinates, *i.e.* a range in $\mathbf{e_x}, \mathbf{e_y}, \mathbf{e_z}$, and a *spherical* one where the region is defined using spherical coordinates , *i.e.* a range in $\mathbf{e_r}, \mathbf{e}_\theta, \mathbf{e}_\phi$.

The detector is therefore a set of cells inside a delimited region, it may be one, two or three-dimensional, and may be defined on a temporal domain as well.

The algorithm loops through the trajectory, calculating the emitted radiation at each step and depositing it in the correct time slot of the detector. In the end, the code returns a file that contains information about the radiation that hit each cell of the detector at each time slot. An example can be found on Figure 2, where we show the state of a 2-D spherical detector at 3 different time steps, after an helically moving particle deposited its radiation.

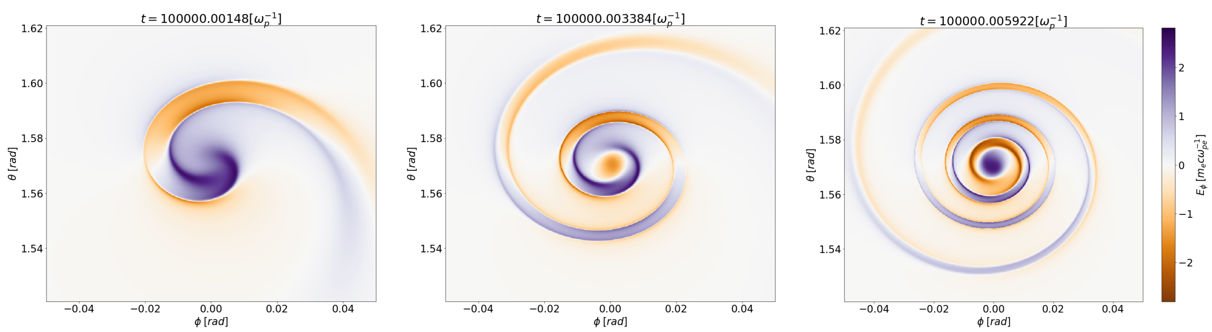

Figure 2: *Evolution of the Electric field at the detector. This is a spherical detector located far from the simulation domain (10^5 $[c/\omega_p]$) where a single particle describes an helical trajectory. The detector has 512 cells along the e_θ direction, and 512 cells along the e_ϕ direction.*

Benchmarking

We benchmarked the results against theoretical expectations found in [5]. According to [5] the angular and frequency distribution of the radiated intensity ($dI(\omega)/d\Omega$) at a spherical surface for a single electron undergoing an helical-like motion is given by:

$$\frac{dI(\omega)}{d\Omega} = \frac{e^2\omega^2K^2}{\pi^2 c\omega_0^2\gamma^2} \sum_{n=-\infty}^{\infty} \left[J_n'^2(x) + \left(\frac{\gamma\theta}{K} - \frac{n}{x} \right)^2 J_n^2(x) \right] \frac{\sin^2\left[N\pi(\omega/\omega_1 - n)\right]}{(\omega/\omega_1 - n)^2} \tag{2}$$

with e being the charge of the electron, c the speed of light, ω_0 the frequency of the helical trajectory, γ the electron's Lorentz factor, K a parameter related to the shape of the helical trajectory, given by $K = |p_\perp|/m_e c$, N the number of periods in the helical trajectory, θ the observation angle, x and ω_1 auxiliary variables given by $x = K\omega\theta/\gamma\omega_0$ and $\omega_1 = 2\gamma^2\omega_0/(1 + K^2 + \gamma^2\theta^2)$. J_n and J_n' are the nth-order Bessel function and its derivative.

The angular and frequency distribution can be retrieved from the code's results by performing a Fourier Transform, as $dI(\omega)/d\Omega \propto |\mathscr{F}(E_x)|^2 + |\mathscr{F}(E_y)|^2 + |\mathscr{F}(E_z)|^2$. In this way, using the spherical version of the code on an helical trajectory with $K = 0.8$ we were able to compare the match the results to the theoretical expectations. Below, in Figure 3 we show a comparison between the obtained results and the theoretical expectations.

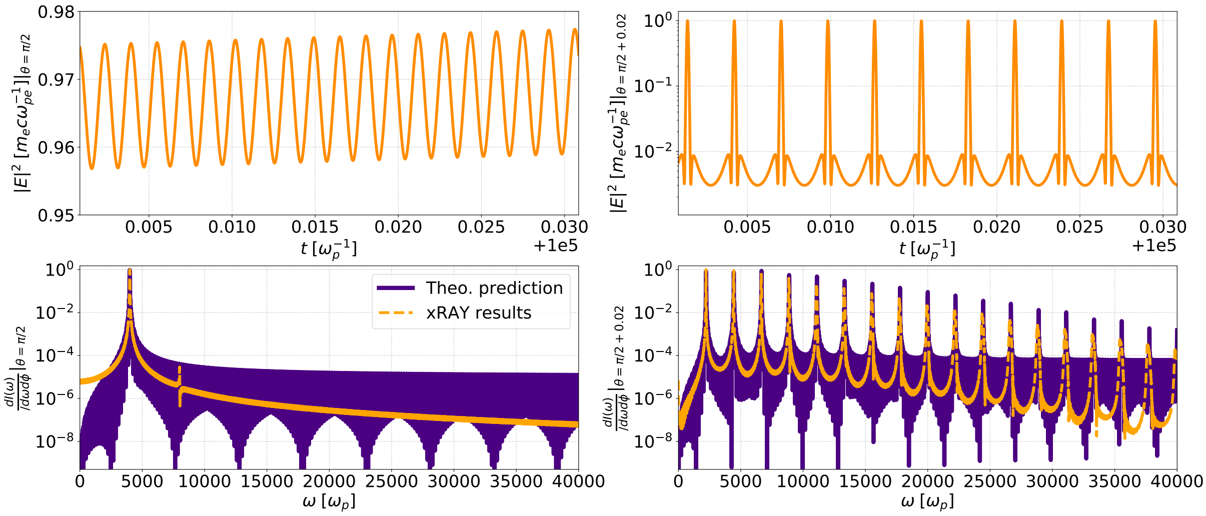

Figure 3: *Benchmarking with the theoretical predictions, the detector is the same as used in the example of Figure 2. The upper plots display the time signature of the electric field at two different locations, both with$\phi = 0$. The lower plots display the Fourier transform of those signals*

Figure 3 shows an almost perfect match between the Fourier transform of the signal left at the detector by the radiation and the theoretical prediction, as all the harmonics appear at the correct frequencies. This a satisfying result as it shows that the code is able to reproduce thrustwortily the features of the emitted radiation which cannot be captured in current PIC codes.

Multiparticle tests

The code is also able to deal with sets of multiple trajectories in parallel. The full set of all trajectories is distributed between the available CPU's using MPI and a copy of the detector is assigne do each CPU. This results in an almost communicationless algorithm with decent scalabily. If the available CPU's support multithreading, the detector's domain can also be split using OpenMP, which helps speeding up the process even more. Below, we show an example of a run with 192 particles with a spherical detector on Figure 4.

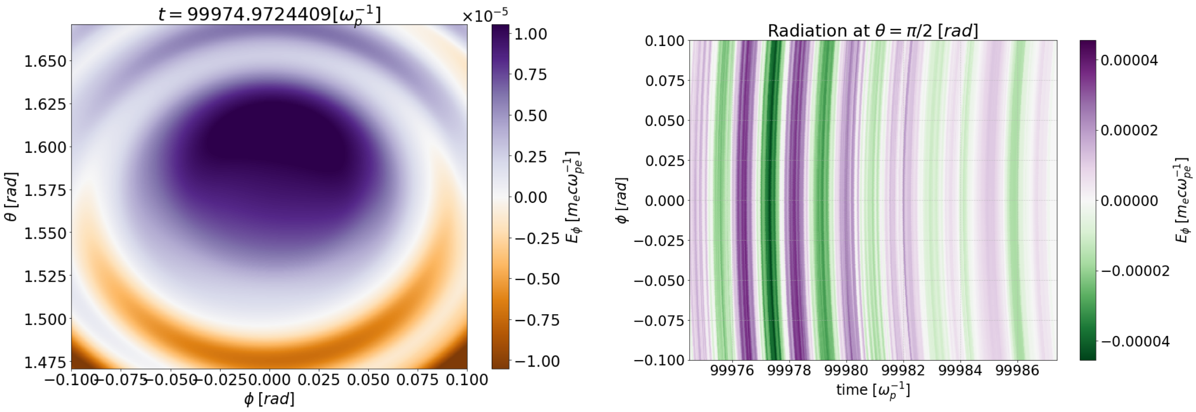

Figure 4: *Spherical detector resutlts for a multiparticle test. The full 1024x1024 detector is shown on the left at a fixed time step, whereas the time evolution of a slice of the detector is shown on the right.*

Conclusion

We developed a post-processing radiation diagnostic [6], that is able to capture the radiation emitted by particles using trajectory files from particle-in-cell codes such as OSIRIS [7].

This diagnostic stores the radiation that hits a finite region of space and time (detector), which gives the user direct access to the spatiotemporal properties of the emitted radiation, with built-in spatiotemporal coherence.

The results were successfully benchmarked against theoretical expectations regarding the spectral content of the radiation emitted by a single particle in helical motion, prooving that the code yields a thrustworthy radiation diagnostic.

References

[1] J. L. Martins *et al.*, Proc. to SPIE **7359**, (2009)

[2] S. Hell *et al.*, Optics Letters **11**, 780-782, (1994)

[3] F. Tamburini, *et al.*, Nature Physics **7**, 195-197 (2011)

[4] J. D. Jackson, Classical Electrodynamics, chapter 14. 3rd ed., (1999)

[5] B. M. Kincaid , Journal of Applied Physics **48**, (1977)

[6] M. Pardal *et al.* to be submitted, (2018)

[7] R. Fonseca *et al.*, LNCS **2331**, (2002)